Hindawi
Mathematical Problems in Engineering
Volume 2022, Article ID 4025831, 14 pages
https://doi.org/10.1155/2022/4025831

Research Article

Unsteady MHD Tangent Hyperbolic Nanofluid Past a Wedge Filled with Gyrotactic Micro-Organism

S. M. Atif,[1] Abdul Hamid Ganie,[2] Ilyas Khan ,[3] and M. Andualem [4]

[1]*Department of Mathematics, Roots School System DHA-1, Islamabad, Pakistan*
[2]*Basic Sciences Department, College of Science and Theoretical Studies, Saudi Electronic University, Abha, Male 61421, Saudi Arabia*
[3]*Department of Mathematics, College of Science Al-Zulfi, Majmaah University, Al-Majmaah, Saudi Arabia*
[4]*Department of Mathematics, Bonga University, Bonga, Ethiopia*

Correspondence should be addressed to Ilyas Khan; i.said@mu.edu.sa and M. Andualem; mulugetaandualem4@gmail.com

Received 28 October 2021; Revised 11 January 2022; Accepted 12 April 2022; Published 12 May 2022

Academic Editor: Mohammadreza Safaei

In this numerical investigation, tangent hyperbolic nanofluid past a wedge-shaped surface filled with gyrotactic micro-organisms has been examined. The simulations have been performed in the presence of Ohmic heating and linear thermal radiation effect. After using similarity transformation to convert modeled PDEs into ODEs, the system of ODEs is tackled with the aid of shooting technique. For the authenticity of the code, the present numerical data have been compared with the already existing results in the literature. The impact of important governing parameters on velocity, concentration, temperature, and motile density distribution is examined graphically. Furthermore, the numerical values of the surface drag, heat transfer rate, mass transfer rate, and motile density number are computed and represented in the tabular form. Our simulations indicate that the Nusselt number is enhanced for the growing values of unsteadiness and the velocity ratio parameters. Moreover, a significant raise in nanofluid velocity is observed as magnetic number gets bigger whereas the temperature profile is depressed. For the above proposed model, it can be concluded that heat and mass can be enhanced by using gyrotactic micro-organism.

1. Introduction

Over the years, the enhancement of the thermal conductivity via nanofluids which upsurge the conductivity of conventional fluids has received considerable attention. In this regard, massive theoretical and experimental work have been done and become the most appealing area of the researchers. A significant enhancement in thermal efficiency of nanofluid due to the presence of nanoparticles as compared with ordinary base fluid was observed by Choi [1] in 1995. Thermal conductivity of nanofluid with copper and aluminium oxide nanoparticles was assessed by Lee et al. [2] and Eastman et al. [3]. Sheikholeslami et al. [4] analyzed the numerical solution of alumina nanofluid with MHD effects in a permeable medium. A major finding was that the average Nusselt number is boosted as the Hartmann number is hiked. Goodarzi et al. [5] studied the heat transfer in the nanofluid with Cu, MWCNT, and Al_2O_3 nanoparticles in a cavity with different aspect ratios and concluded that the heat transfer in the cavity is influenced by fluid circulation caused by natural convection and conductive heat transfer mechanism. By considering variable viscosity and thermal radiation, Mondal et al. [6] discussed the magnetohydrodynamic dusty nanofluid. An augmentation in surface drag was noticed for strengthening parametric values of thermophoresis while a decrement in the Nusselt number was observed in accordance with larger Brownian motion parameter. Khamliche et al. [7] ascertained the enhancement of the thermal conductivity of silver nanoparticles with ethylene glycol as based fluid. Their concluding remark was that the thermal conductivity is enhanced by 23% due to addition of 0.1% volume and temperature of 50°C for the Ag nanowires in ethylene glycol as base fluid. Nisar et al. [8] studied the Eyring Powell nanofluid in peristaltic transport with activation energy and reported that the concentration distribution was declined as the activation energy parameter is upsurged. Ellahi et al. [9] investigated two-phase Newtonian hybrid nanofluid flow with Hafnium Particles and slip effects. One of the key observations was that the velocity profile was declined as the Hartmann number is hiked. In a liquid microlayer inside a microreactor, production of the heat transfer by plasmon was reported by Sarafraz and Christo [10]. They concluded that the strongest phase change occurred at light wavelength of 680 nm. Heat transfer in MHD boundary layer flow past a wedge with viscous effects and porous media was ascertained by Ibrahim and Tulu [11]. Atif et al. [12] studied MHD tangent hyperbolic nanofluid past a wedge. Effects of thermal radiation, internal heat generation, and buoyancy on velocity and heat transfer in the Blasius flow were reported by Ibrahim et al. [13]. One of the main conclusions was that the temperature profile declines as the Grashof number is heightened. For further details, refer [14–23].

The non-Newtonian fluids which are electrically conducting allied with a magnetic field have wide-ranging applications in numerous fields like pharmaceutical and hydrometallurgical industry. This has generated a keen interest among the modern day researchers. MHD is widely used to modify the flow field in the desired directions. MHD tangent hyperbolic fluid flow over a stretching cylinder was reported by Malik et al. [24]. It was noticed that the increment in magnetic parameter upturns the resistance to the fluid flow. Ellahi et al. [25] presented the MHD and slip effects on heat transfer boundary layer flow over a moving plate based on specific entropy generation. Jabeen et al. [26] explored the MHD boundary layer flow caused by nonlinear stretching surface in the presence of the porous medium. It was obtained that the velocity profile on increasing magnetic parameter increases whereas the other two profiles, namely, thermal and concentration show the reverse trends for increasing magnetic parameter. Ramzan et al. [27] ascertained the Hall and Ion slip effects in 3D tangent hyperbolic nanofluid. Gharami et al. [28] explored the MHD unsteady flow using the tangent hyperbolic nanofluid model along with chemical reaction and thermal radiation effects. It was concluded that the Nusselt number and skin friction closer to the wall subsided for the higher values of magnetic and thermophoretic parameters. Effect of zero mass flux conditions on tangent hyperbolic nanofluid was studied by Shafiq et al. [29]. Numerical study of momentum and heat transfer of MHD Carreau nanofluid over exponentially stretched plate with internal heat source/sink and radiation was studied by Yousif et al. [30]. An extensive literature on the flow of the MHD tangent hyperbolic fluid model considering different effects over different geometries can be seen in [31–37].

The motile micro-organisms which are self-propelled are added in order to increase the suspensions stability. These micro-organisms rise the base fluid density in response to additional stimulant. Xu and Cui [38] investigated the mixed convective flow under the slip effects and porous medium containing nanoparticles and micro-organisms and found that the variation in the Reynolds number alters all the quantities of physical interest. Pal and Mondal [39] discussed the effect of nonlinear thermal radiation and chemical reaction on bioconvective MHD nanofluid flow with gyrotactic micro-organisms in an exponential stretching sheet. A major finding was that the nanoparticles concentration is enhanced as the chemical reaction parameter is boosted. Atif et al. [40] studied the MHD micropolar nanofluid with gyrotactic micro-organisms. Linear stability of bioconvection nanofluid was performed by Zhao et al. [41] and noticed that the suspension becomes unstable if the thermal Raleigh number is increased to 1750. Saini and Sharma [42] reported that the intermediate swimmers have destabilizing effect, and for smaller values of the wave number, the subcritical region of instability becomes large. Recently, Al-Khaled et al. [43] explored the nonlinear thermal radiation effects on the flow of the bioconvective tangent hyperbolic nanofluid model with chemical reaction. This study revealed that the rate of heat transfer is enhanced for higher thermophoretic parameter.

In fluid dynamics boundary layer, wedge flow is a classic problem and is presented everywhere in fluid dynamics. It can be seen in manufacturing units, industrial processes, or the design of prototypes for technological advancements in aerospace or defense laboratories. Application of the wedge flow could be found in molten metals flow over a ramped surface nuclear power plants, flow of chilled air through AC panels, designing of flaps on airplane wings for the enhancement of the lift, manoeuvre and drag, modeling of warships, submarines, and in several other domains of science and engineering. In fact, wedge angle plays a crucial role in the study of transonic flows over airfoils and wings, including flows at Mach 1 [44].

On analyzing the all existing reports, it is noticed that no one has studied the non-Newtonian tangent hyperbolic nanofluid in the presence of gyrotactic micro-organism yet. The prime objective of this study is to investigate theoretically, the effect of Ohmic heating, magnetic parameter, and linear thermal radiation on tangent hyperbolic nanofluid flow over a wedge-shaped body filled with gyrotactic micro-organisms. The equations which govern the flow and heat transfer are numerically solved via a numerical technique called shooting method. The variation due to important parameters of physical interest involved in the governing system of equations are studied graphically and discussed in detail. The influence of the important parameters on skin friction, Nusselt number, Sherwood number, and motile density number has been studied and presented in the form of tables. Moreover, for the authenticity of the shooting code, numerical values of the skin friction coefficient which were already reported in the literature have been reproduced.

2. Problem Formulation

Two-dimensional unsteady tangent hyperbolic fluid flow in the presence of nanoparticles past a wedge surface has been analyzed. For the stability of the nanofluid, self-propelled micro-organism is considered. The stretching velocity of the wedge is considered as velocity $U_w(x,t) = bx^m/1 - ct$. The

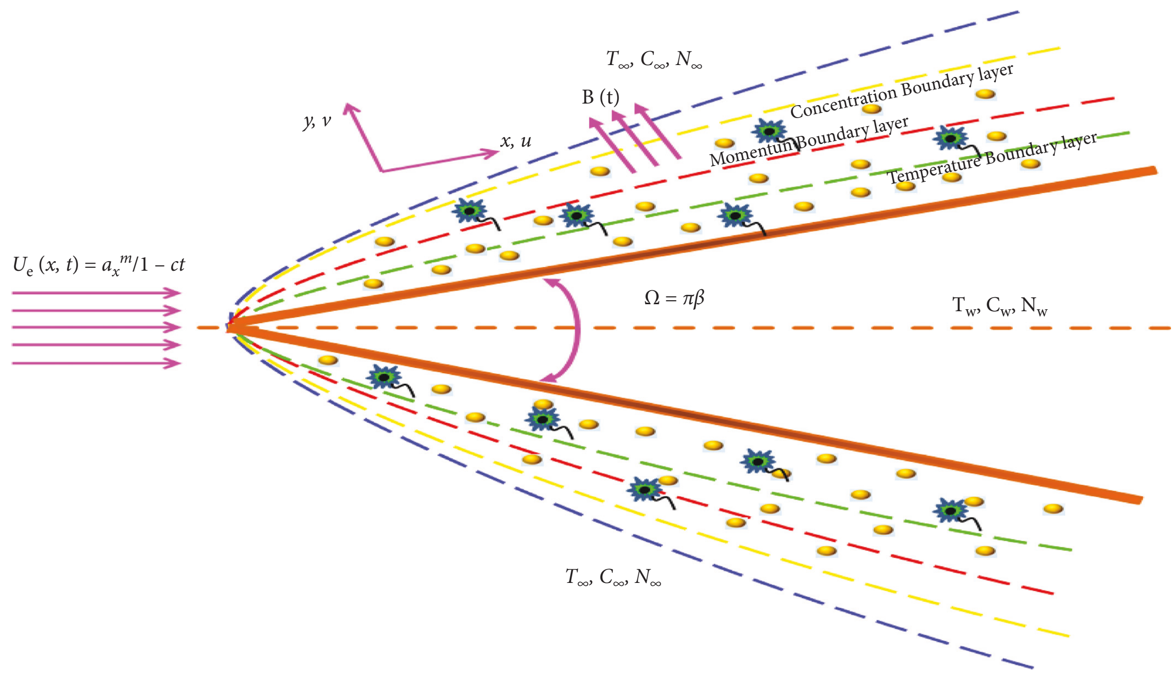

FIGURE 1: Flow configuration.

nose shaped object is placed along $x-$axis and $y-$axis and is perpendicular to the wedge as illustrated in Figure 1. The free stream velocity is assumed as $U_e(x,t) = ax^m/1 - ct$ with $0 \leq m \leq 1$, and m, a, and c are constants. The surface temperature, surface nanoparticles concentration, and surface micro-organism's concentration are defined as $T_w(x,t) = T_\infty + T_0 U_w x/\nu(1-ct)^{1/2}$, $C_w(x,t) = C_\infty + C_0 U_w x/\nu(1-ct)^{1/2}$, and $N_w(x,t) = N_\infty + N_0 N_w x/\nu(1-ct)^{1/2}$, respectively. Time-dependent magnetic field $B(t) = B_0/(1-ct)^{1/2}$ perpendicular to wedge has also been considered. Induced magnetic field is negligible due to the assumption of the small magnetic Reynolds number.

2.1. Assumptions and Constraints

(1) 2D laminar unsteady flowing
(2) Boundary layer estimation
(3) Non-Newtonian tangent hyperbolic fluid
(4) Ohmic heating
(5) Buongiorno model
(6) Small Reynolds number
(7) Thermal radiative flow

Under the above assumptions, the governing equations of the above modeled problem are as follows [40–50]:

$$\begin{aligned}
&\frac{\partial u}{\partial x} + \frac{\partial v}{\partial y} = 0,\\
&\frac{\partial u}{\partial t} + u\frac{\partial u}{\partial x} + v\frac{\partial u}{\partial y} = \frac{\partial U_e}{\partial t} + U_e\frac{\partial U_e}{\partial x} + \nu\left((1-n) + \sqrt{2}\,n\Gamma\frac{\partial u}{\partial y}\right)\frac{\partial^2 u}{\partial y^2} - \frac{\sigma B_0^2}{\rho}(u - U_e),\\
&\frac{\partial T}{\partial t} + u\frac{\partial T}{\partial x} + v\frac{\partial T}{\partial y} = \alpha\frac{\partial^2 T}{\partial y^2} - \frac{1}{\rho C_p}\frac{\partial q_r}{\partial y} + \Lambda\left[D_B\frac{\partial C}{\partial y}\frac{\partial T}{\partial y} + \frac{D_T}{T_\infty}\left(\frac{\partial T}{\partial y}\right)^2\right] + \frac{\sigma}{\rho C_p}B_0^2(u - U_e)^2,\\
&\frac{\partial C}{\partial t} + u\frac{\partial C}{\partial x} + v\frac{\partial C}{\partial y} = \frac{D_T}{T_\infty}\frac{\partial^2 T}{\partial y^2} + D_B\frac{\partial^2 C}{\partial y^2},\\
&\frac{\partial N}{\partial t} + u\frac{\partial N}{\partial x} + v\frac{\partial N}{\partial y} = D_n\frac{\partial^2 N}{\partial y^2} - \frac{bW_c}{C_w - C_\infty}\left(\frac{\partial N}{\partial y}\frac{\partial C}{\partial y} + N\frac{\partial^2 C}{\partial y^2}\right).
\end{aligned} \tag{1}$$

The associated BCs are as follows:

$$\left.\begin{array}{l}\text{for } y = 0 \ u = U_w = \lambda U_e, v = 0, T = T_w(x,t), C = C_w(x,t), N = N_w(x,t), \\ \text{as } y \longrightarrow \infty \ u \longrightarrow U_e, T \longrightarrow T_\infty, C \longrightarrow C_\infty \ N \longrightarrow N_\infty.\end{array}\right\} \tag{2}$$

For the dimensionless equations, the following transformations [45] have been considered:

$$\left.\begin{array}{l}\eta = y\sqrt{\dfrac{(m+1)U_e}{2\nu x}}, \\ \psi = \sqrt{\dfrac{2\nu x U_e}{m+1}} f(\eta), \\ \xi(\eta) = \dfrac{N - N_\infty}{N_w - N_\infty}, \\ \phi(\eta) = \dfrac{C - C_\infty}{C_w - C_\infty}, \\ \theta(\eta) = \dfrac{T - T_\infty}{T_w - T_\infty}.\end{array}\right\}. \tag{3}$$

With the application of the similarity transformation, the continuity equation is automatically satisfied and the transformed ODEs [12, 45, 48–50] are as follows:

$$(1 - n + nWef'')f''' - (2-\beta)\left[A\left(\frac{\eta}{2}f'' + f' - 1\right) + M(f' - 1)\right] - \beta\left(f'^2 - 1\right) + ff'' = 0, \tag{4}$$

$$\left(1 + \frac{4}{3}Rd\right)\theta'' - \Pr\left[(2f'\theta - f\theta') + \frac{A}{2}(2-\beta)(\eta\theta' + 3\theta) - Nb\theta'\phi' - Nt\theta'^2 - EcM(2-\beta)(f' - 1)^2\right] = 0, \tag{5}$$

$$\phi'' + Sc(f\phi' - 2f'\phi) - Sc\frac{A}{2}(2-\beta)(\eta\phi' + 3\phi) + \frac{Nt}{Nb}\theta'' = 0, \tag{6}$$

$$\xi'' - Pe(\xi'\phi' + (\xi + \beta^*)\phi'') - Lb[A(2-\beta)(\eta\xi' + 3\xi) + (2f'\xi - f\xi')] = 0. \tag{7}$$

The BCs after using transformations are

$$\left.\begin{array}{l}\text{for } \eta = 0 \ f(\eta) = 0, f'(\eta) = \lambda, \theta(\eta) = 1, \phi(\eta) = 1, \xi(\eta) = 1 \\ \text{as } \eta \longrightarrow \infty \ f'(\eta) \longrightarrow 1, \theta(\eta) \longrightarrow 0, \phi(\eta) \longrightarrow 0, \xi(\eta) = 0.\end{array}\right\} \tag{8}$$

3. Quantities of Interest

In this section, the dimensional and dimensionless forms of the skin friction, Nusselt, Sherwood, and density numbers are presented.

$$\begin{aligned}C_f &= \frac{\tau_w}{\rho u_w^2}, \\ Nu_x &= \frac{xq_w}{k(T_w - T_0)}, \\ Sh_x &= \frac{xq_m}{D_B(C_w - C_0)}, \\ Nn_x &= \frac{xq_n}{D_n(N_w - N_0)}.\end{aligned} \tag{9}$$

In dimensionless form, these quantities are as follows:

$$\left.\begin{aligned}&C_f \mathrm{Re}_x^{1/2}\sqrt{\frac{2}{m+1}} = \left(1-n+\frac{n}{2}Wef''(0)\right)f''(0),\ Sh_x \mathrm{Re}_x^{-1/2}\sqrt{\frac{2}{m+1}} = -\phi'(0)\\ &Nu_x \mathrm{Re}_x^{-1/2}\sqrt{\frac{2}{m+1}} = -\left(1+\frac{4}{3}Rd\right)\theta'(0).\ Nn_x \mathrm{Re}_x^{-1/2}\sqrt{\frac{2}{m+1}} = -\xi'(0),\end{aligned}\right\} \tag{10}$$

where $Re_x = xU_e/\nu$.

4. Numerical Treatment

4.1. Shooting Technique. The solution of the coupled system of equations (4)–(7) along with BCs equation (8) is achieved with the help of shooting technique.

Now, we introduce new variables $\Psi_1 = f, \Psi_2 = f'$, $\Psi_3 = f''$, $\Psi_4 = \theta$, $\Psi_5 = \theta'$, $\Psi_6 = \phi$, $\Psi_7 = \phi'$, $\Psi_8 = \xi$, and $\Psi_9 = \xi'$.

The system equations and associated boundary conditions are of the form as follows:

$$\left.\begin{aligned}&\Psi_1' = \Psi_2,\\ &\Psi_2' = \Psi_3,\\ &\Psi_3' = \frac{1}{1-n+nWe\Psi_3}\left[(2-\beta)A\left(\frac{\eta}{2}\Psi_3+\Psi_2-1\right)+\beta\left(\Psi_2^2-1\right)-\Psi_1\Psi_3+M(2-\beta)(\Psi_2-1)\right]\Psi_4' = \Psi_5,\\ &\Psi_5' = \frac{-3\mathrm{Pr}}{(3+4Rd)}\left[\Psi_1\Psi_5-2\Psi_2\Psi_4-\frac{A}{2}(2-\beta)(\eta\Psi_5+3\Psi_4)+Nb\,\Psi_5\Psi_7+Nt\,\Psi_5^2+Ec\,M(2-\beta)(\Psi_2-1)^2\right]\Psi_6' = \Psi_7,\\ &\Psi_7' = Sc\left(\frac{A}{2}(2-\beta)(\eta\Psi_7+3\Psi_6)-(\Psi_1\Psi_7-2\Psi_2\Psi_6)\right)-\frac{Nt}{Nb}\Psi_5', \Psi_8' = \Psi_9,\\ &\Psi_9' = Pe\left(\Psi_9\Psi_7+(\Psi_8+\beta^*)\Psi_7'\right)+Lb\left[A(2-\beta)(\eta\Psi_9+3\Psi_8)+2\Psi_2\Psi_6-\Psi_1\Psi_9\right],\end{aligned}\right\} \tag{11}$$

with BCs

$$\left.\begin{aligned}&\text{For } \eta = 0\ \Psi_1(\eta) = 0, \Psi_2(\eta) = \lambda\ \Psi_4(\eta) = 1, \Psi_6(\eta) = 1, \Psi_8(\eta) = 1,\\ &\text{As } \eta \longrightarrow \infty\ \Psi_2(\eta) \longrightarrow 1, \Psi_4(\eta) \longrightarrow 0, \Psi_6(\eta) \longrightarrow 0, \Psi_8(\eta) \longrightarrow 0.\end{aligned}\right\} \tag{12}$$

Unknown initial conditions $\Psi_3(0) = s_1$, $\Psi_5(0) = s_2$, $\Psi_7(0) = s_3$, and $\Psi_9(0) = s_4$ are considered to satisfy the known BCs. Initial guesses s_1, s_2, s_3, and s_4 are refined with the help of Newton's iterative scheme until defined criteria are not achieved. In order to stop the iterative process, following criteria are assumed:

$$\begin{aligned}&\max\left\{\left|\Psi_2(\eta_{\max})-1\right|, \left|\Psi_4(\eta_{\max})-0\right|,\right.\\ &\left.\cdot\left|\Psi_6(\eta_{\max})-0\right|, \left|\Psi_8(\eta_{\max})-0\right|\right\} < 10^{-10}.\end{aligned} \tag{13}$$

We have considered a bounded domain $[0,\infty]$ instead of $[0,\infty)$ for the numerical computations. From our computational experience, it is noticed that boosting $\eta_{\max}$, no substantial fluctuations are noticed in the computational results.

4.2. Flow Chart. Flow chart is shown in Figure 2.

4.3. Code Verification. For the correctness and verification of the MATLAB code, the skin friction values $-f''(0)$ which were reported in the literature by Rajagopal et al. [48], Kuo [49], and Ishak et al. [50] have been reproduced. Our computational results have an admirable agreement with their results (Table 1).

5. Results and Discussion

5.1. The Skin Friction Coefficient. Table 2 is prepared to study the fluctuation in the skin friction coefficient due to the Weissenberg number We, unsteadiness parameter A, velocity ratio parameter λ, power law index n, Hartree pressure gradient β, and magnetic parameter M. Our simulations depict that the skin friction coefficient $Re_x^{-1/2}C_f\sqrt{2/m+1}$ is vitiated for the higher values of velocity ratio parameter λ and power law index n while a hike up is observed for enhancing

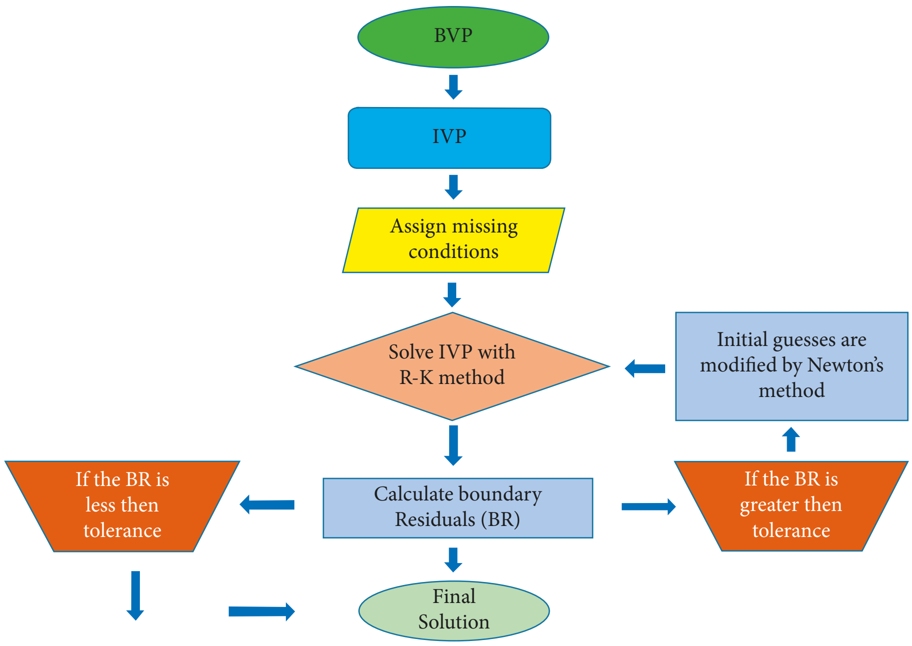

FIGURE 2: Flow chart.

TABLE 1: Numerical data of the computed values of $-f''(0)$ [48–50].

β	[48]	[49]	[50]	Present study
0.0	—	0.469600	0.4696	0.469600
0.1	0.587035	0.587080	0.5870	0.587035
0.3	0.774755	0.774724	0.7748	0.774755
0.5	0.927680	0.927905	0.9277	0.927680
1.0	1.232585	1.238589	1.2326	1.232588
1.6	1.521514	1.518488	1.5215	1.521551

TABLE 2: Numerical values of $C_f \mathrm{Re}^{1/2}\sqrt{2/m+1}$ when $Lb = Rd = 1, \beta^* = Pe = Ec = Sc = 0.2, Pr = 7$, and $Nt = Nb = 0.1$.

A	n	We	M	β	λ	$C_f \mathrm{Re}^{1/2}\sqrt{(2/m+1)}$
0.2	0.2	1	0.1	0.1	0.3	0.618741
0.3						0.662672
0.4						0.705045
0.2	0.3					0.591906
	0.5					0.537024
	0.7					0.480843
	0.2	0.5				0.609744
		2				0.635470
		3				0.650840
		1	0.1			0.618741
			0.3			0.737507
			0.5			0.841418
			0.1	0.2		0.661328
				0.4		0.739924
				0.6		0.811700
				0.1	0.2	0.691738
					0.4	0.541350
					0.6	0.374491

Table 3: Numerical values of $\mathrm{Re}_x^{-1/2} Nu_x \sqrt{2/m+1}$ for various parameters when $Lb = 1, n = 0.2, We = 1$, and $Sc = \beta^* = Pe = 0.2$.

A	Rd	Nb	Nt	M	Pr	β	Ec	λ	$Re_x^{-1/2} Nu_x \sqrt{(2/m+1)}$
0.1	1	0.1	0.1	0.1	7	0.1	0.2	0.3	4.264843
0.2									4.638632
0.3									4.989138
0.2	2								6.048218
	3								7.244505
	4								8.306865
	1	0.2							4.448489
		0.4							4.089907
		0.6							3.760368
		0.1	0.2						4.472414
			0.4						4.161547
			0.6						3.878221
			0.1	0.2					4.643489
				0.3					4.646502
				0.4					4.648149
				0.1	7				4.638676
					10				5.361452
					15				6.298947
					1	0.2			4.627500
						0.4			4.600568
						0.6			4.568220
						0.1	0.4		4.610188
							0.6		4.582073
							0.8		4.553956
							0.2	0.2	4.309568
								0.4	4.949331
								0.6	5.526109

Table 4: The numerical values $-\mathrm{Re}_x^{-1/2} Sh_x \sqrt{2/m+1}$ for various parameters when $Lb = Rd = We = 1, Pr = 7$, and $\beta^* = Pe = Ec = n = 0.2$.

A	Nb	Nt	M	β	λ	$-Re_x^{-1/2} Sh_x \sqrt{(2/m+1)}$
0.1	0.1	0.1	0.1	0.1	0.3	0.726523
0.2						0.824367
0.3						0.914499
0.2	0.2					0.053217
	0.4					−0.329876
	0.6					−0.329901
	0.3	0.2				0.192495
		0.4				0.870622
		0.6				1.417330
		0.3	0.2			0.541510
			0.3			0.534349
			0.5			0.521425
			0.1	0.2		0.534660
				0.4		0.521431
				0.6		0.508467
				0.1	0.2	0.457287
					0.4	0.636060
					0.6	0.796142

each of Weissenberg number We, unsteadiness parameter A, Hartree pressure gradient β, and magnetic parameter M.

5.2. The Nusselt Number. The fluctuations in the heat transfer rate $Re_x^{-1/2} Nu_x \sqrt{2/m+1}$ caused by variation in important parameters are demonstrated in Table 3. The Nusselt number is enhanced as the values of the Prandtl number Pr, velocity ratio parameter λ, unsteadiness parameter A, the magnetic number M, and thermal radiation parameter Rd are hiked; however, it is depressed as thermophoresis parameter Nt, Hartree pressure gradient β, Brownian motion parameter Nb, and Eckert number Ec are increased.

Table 5: Numerical values of $\mathrm{Re}_x^{-1/2} Nn_x \sqrt{2/m+1}$ for pertinent parameters when $Rd = We = 1, M = 0.1, Pr = 7$, and $A = Ec = n = 0.2$.

β	β^*	Sc	Pe	Lb	Nt	Nb	λ	$\mathrm{Re}_x^{-1/2} Nn_x \sqrt{(2/m+1)}$
0.1	0.2	0.2	0.2	1	0.1	0.1	0.3	1.294224
0.2								1.286385
0.3								1.277968
0.1	0.4							1.260807
	0.6							1.227390
	0.8							1.193973
	0.2	0.5						1.378667
		1						1.470230
		2						1.595195
		1	0.2					1.378667
			0.5					1.243516
			1					1.018624
			0.2	2				2.029791
				3				2.455442
				4				2.812551
				2	0.2			1.892830
					0.4			1.707821
					0.6			1.610277
					0.3	0.2		2.024691
						0.4		2.140621
						0.6		2.176051
						0.3	0.2	2.005064
							0.4	2.196796
							0.6	2.374883

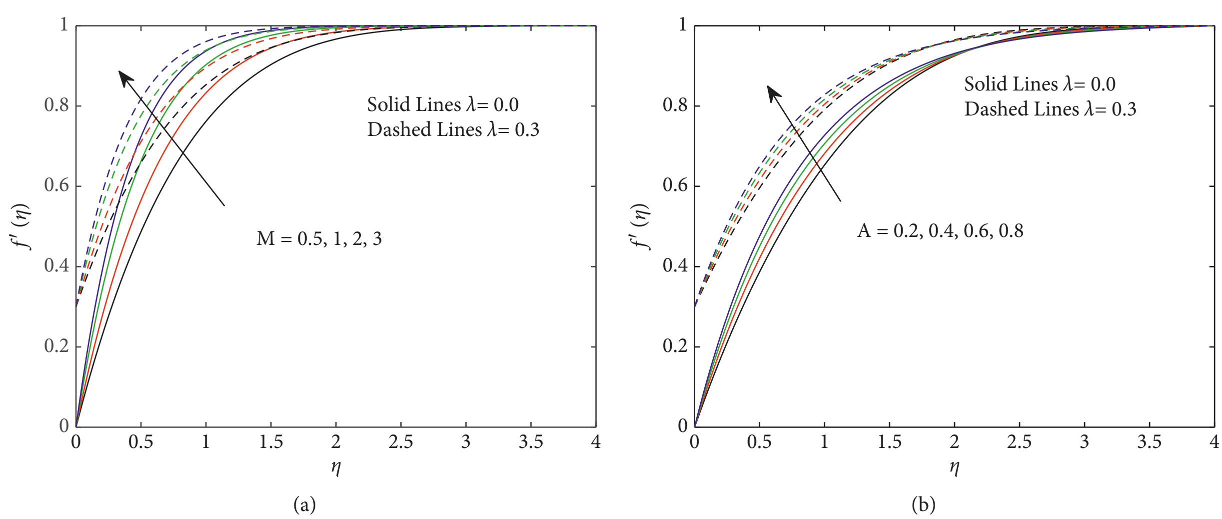

Figure 3: Fluctuations due to (a) M and (b) A in $f'(\eta)$.

5.3. The Sherwood Number. To visualize the fluctuations in the Sherwood number $-Re_x^{-1/2} Sh_x \sqrt{2/m+1}$ due to various pertinent parameters, Table 4 is displayed. The Sherwood number is enhanced for growing values of each of the unsteadiness parameter A, thermophoresis parameter Nt,and velocity ratio parameter λ while it is attenuated for the rising values of the magnetic parameter M, Hartree pressure gradient β, and Brownian motion parameter Nb.

5.4. The Density Number. Table 5 is represented to analyze the fluctuations in the density number $Re_x^{-1/2} Nn_x \sqrt{2/m+1}$ due to physical parameters. The gradually boosting values of the Schmidt number Sc, velocity ratio parameter λ, bio-convection Lewis parameter Lb, and Brownian motion parameter Nb cause an enhancement in the density number while it decreases as the micro-organism concentration difference parameter β^*, thermophoresis parameter Nt, Hartree pressure gradient β and Peclet number Pe are enhanced.

5.5. Graphical Results. In this section, the impact of governing parameters on flow field, energy, concentration, and density profile is sketched and discussed in detail. Both stretching and statics cases have been discussed.

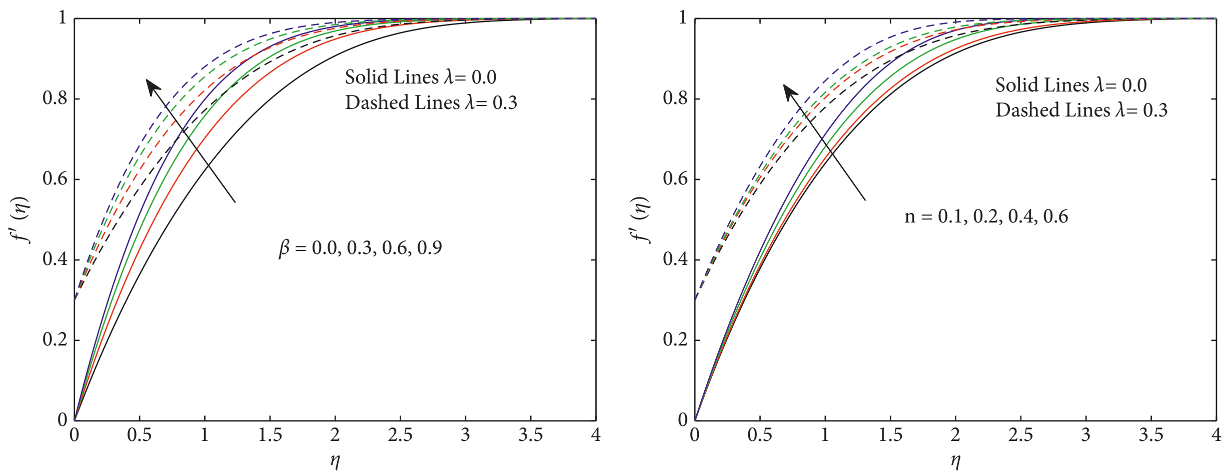

(a) (b)

Figure 4: Fluctuations due to (a) β and (b) n in $f'(\eta)$.

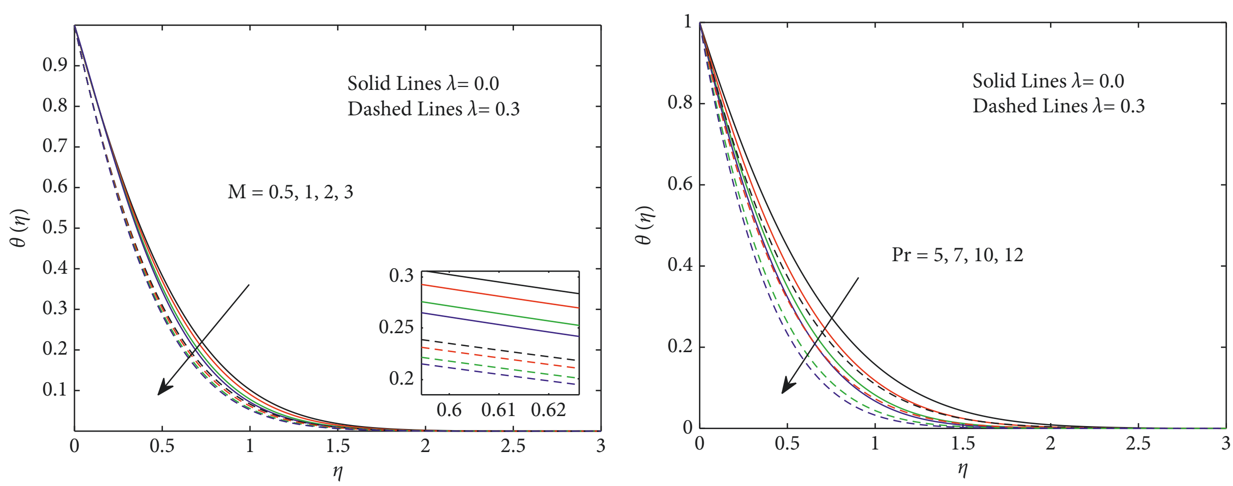

(a) (b)

Figure 5: Fluctuations due to (a) M and (b) Pr in $\theta(\eta)$.

For graphical results, the involved parameters are allocated fixed values as $A = Pe = \beta^* = Ec = n = 0.2$, $We = Lb =, Rd = 1, M = \beta = Nb = Nt = 0.1\mathrm{Pr} = 7$, and $\lambda = 0.3$ unless otherwise mentioned.

5.5.1. The Velocity Profile. To expose the impact of governing parameters on the velocity distribution $f'(\eta)$ of the tangent hyperbolic nanofluid, Figures 3(a), 3(b), 4(a), and 4(b) are displayed. Figures 3(a) and 3(b) are demonstrated to present the fluctuation in $f'(\eta)$ caused by the magnetic number M and unsteadiness parameter A. From this figure, it is evident that velocity profile $f'(\eta)$ is upsurged for the higher values of the magnetic number M and displayed in Figure 3(a). Increment in the magnetic number M means a decrement in the viscous force which lessens the momentum boundary layer thickness. Figure 3(b) is sketched to study the influence of unsteadiness parameter A on velocity profile $f'(\eta)$. The growing values of unsteadiness parameter A and velocity profile $f'(\eta)$ are enhanced whereas related boundary layer thickness becomes thinner. However, in case of stretching wedge, it is higher as compared with the static wedge. The influence of the wedge angle parameter β and power law index n on velocity distribution $f'(\eta)$ is captured in Figures 4(a) and 4(b). $\beta > 0$ addresses the accelerating flow, and it is an interesting fact that the boundary layer thickness is declined as β is hiked and fluid squeezes more closer to the wall surface, as presented in Figure 4(a). Figure 4(b) is divulged to study the impact of the power law index n. This figure shows that velocity profile $f'(\eta)$ is escalated for accelerating values of the power law index n

5.5.2. The Temperature Profile. The impact of sundry parameters on the temperature profile $\theta(\eta)$ is presented in Figures 5–7. Figures 5(a) and 5(b) portray the influence

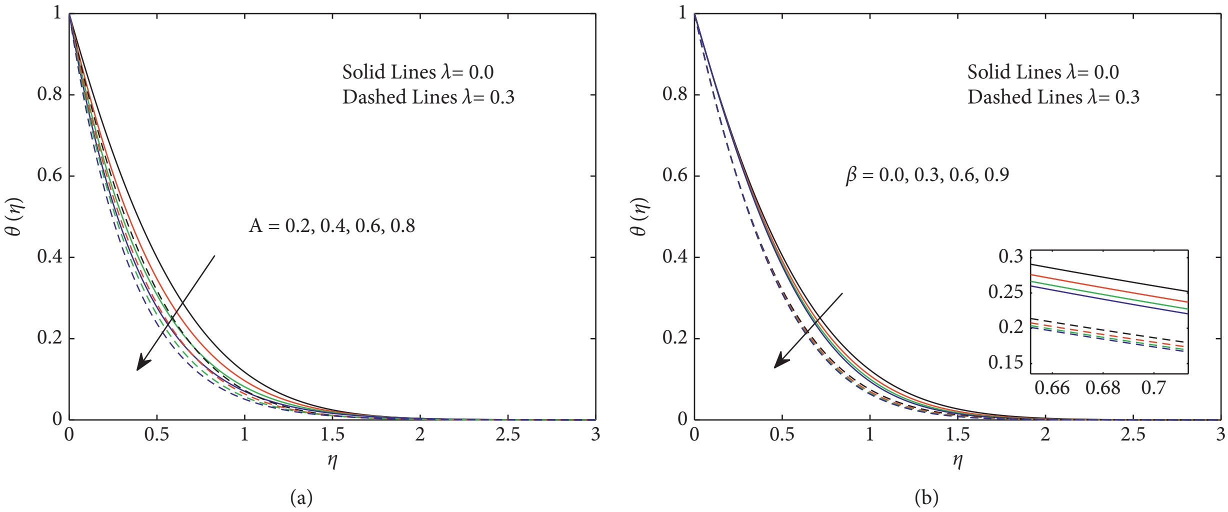

Figure 6: Fluctuations due to (a) A and (b) β in $\theta(\eta)$.

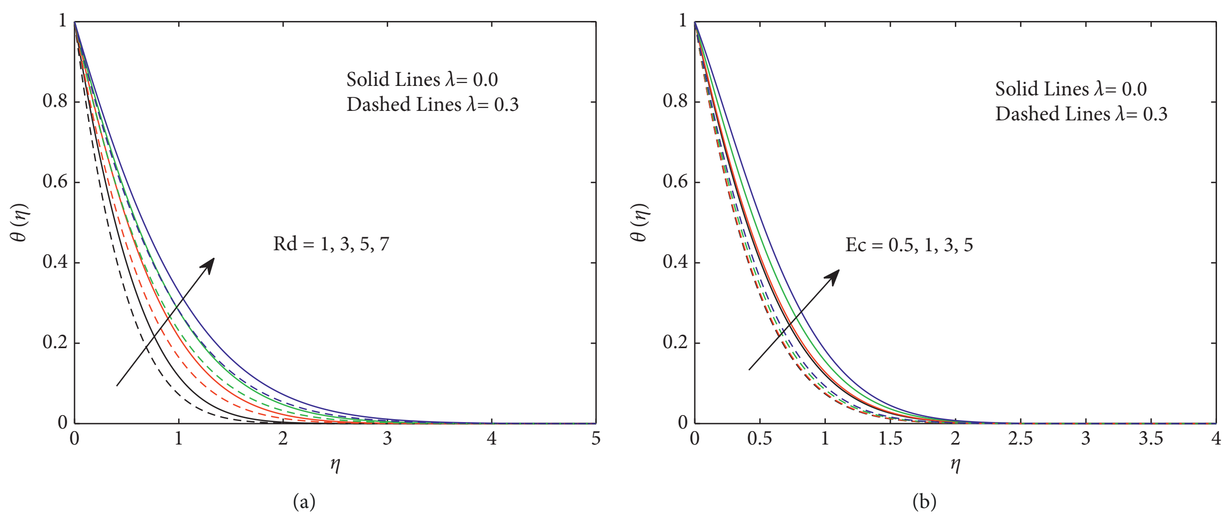

Figure 7: Fluctuations due to (a) Rd and (b) Ec in $\theta(\eta)$.

magnetic number M and Prandtl number Pr on temperature profile $\theta(\eta)$. A decreasing trend is noticed in temperature profile $\theta(\eta)$ as the values of the magnetic number M are escalated as displayed in Figure 5(a). Figure 5(b) reflects the impact Pr on the temperature distribution. The curves in this figure indicate that increasing the Prandtl number Pr causes a decline in the energy profile. Physically, increase in Pr reduces the effect of the thermal conductivity due to which temperature profile $\theta(\eta)$ reduces. Figure 6(a) reflects that the unsteadiness parameter A diminishes the temperature profile $\theta(\eta)$. Physically, when the unsteadiness parameter A is increased, the stretching sheet loses its heat due to which the temperature of the nanofluid is declined. To expose the behavior of β, Figure 6(b) is displayed. For the value $\beta = 0$, the temperature is maximum, and for the growing values of $\beta > 0$, the temperature profile is declined. The temperature distribution $\theta(\eta)$ is escalated as Rd gets bigger as shown in Figure 7(a). Physically, increment in temperature profile $\theta(\eta)$ strengthens the fact that more heat is produced due to the radiation process. The effect of viscous dissipation is presented by Eckert number Ec. It is a number that represents the relation between the kinetic energy and the change in enthalpy. The impact of the Eckert number Ec on temperature profile $\theta(\eta)$ is chalked out in Figure 7(b). It is noticed that as Ec grows, the energy profile $\theta(\eta)$ is boosted. Physically, as the dissipation is increased, the thermal conductivity improves which helps to increase the temperature profile $\theta(\eta)$.

5.5.3. The Concentration Profile. In order to study the variations in concentration distribution $\phi(\eta)$ due to the impact of sundry parameters, Figures 8(a) and 8(b) are presented. Figure 8(a) is chalked out to study the effect of unsteadiness parameter A on $\phi(\eta)$. A decrement in concentration distribution $\phi(\eta)$ is viewed for the higher values of unsteadiness parameter A. Figure 8(b) is demonstrated to view the effect of the Schmidt number Sc on $\phi(\eta)$. As the

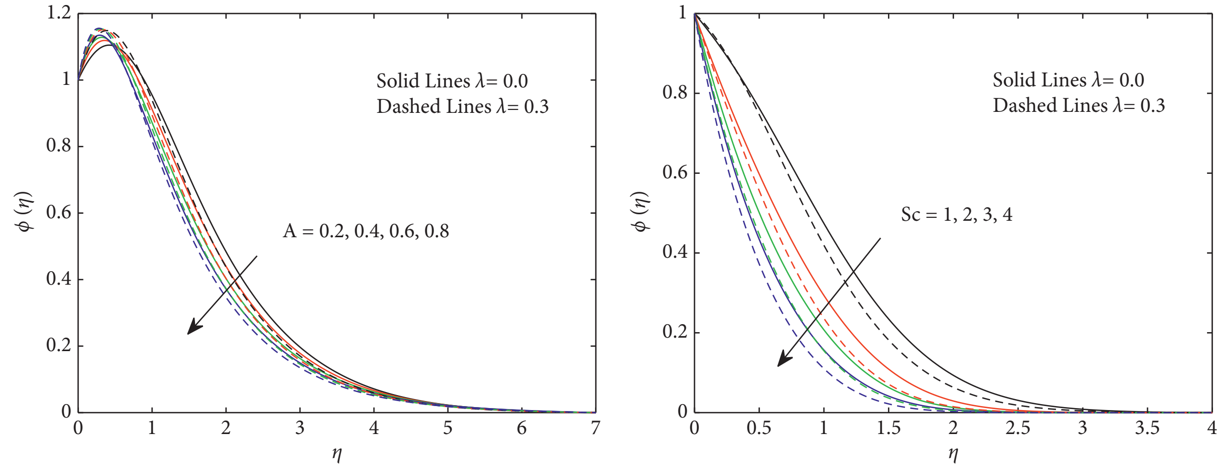

FIGURE 8: Variations due to (a) A and (b) Sc in $\phi(\eta)$.

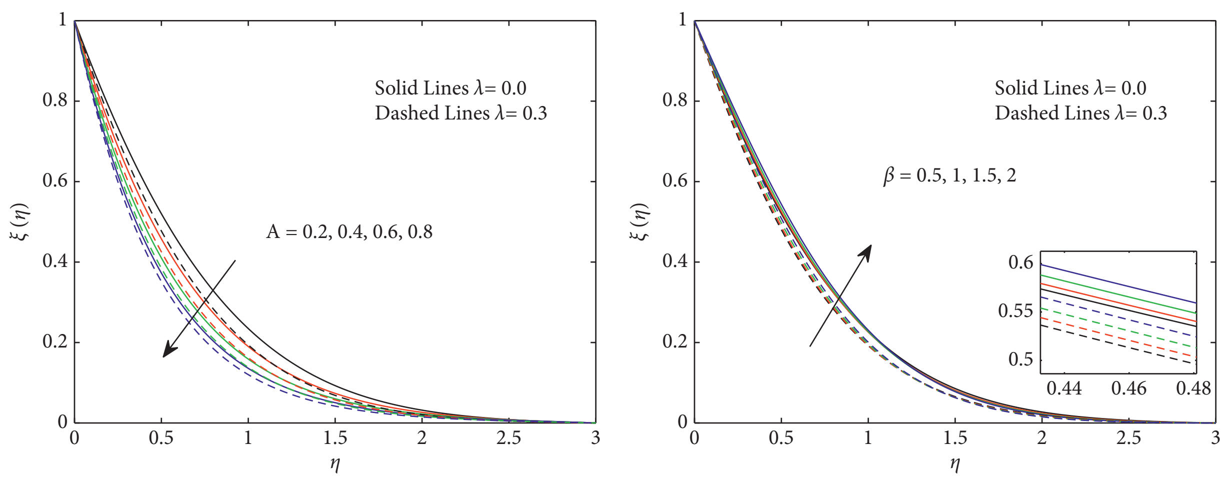

FIGURE 9: Variations due to (a) A and (b) β in $\xi(\eta)$.

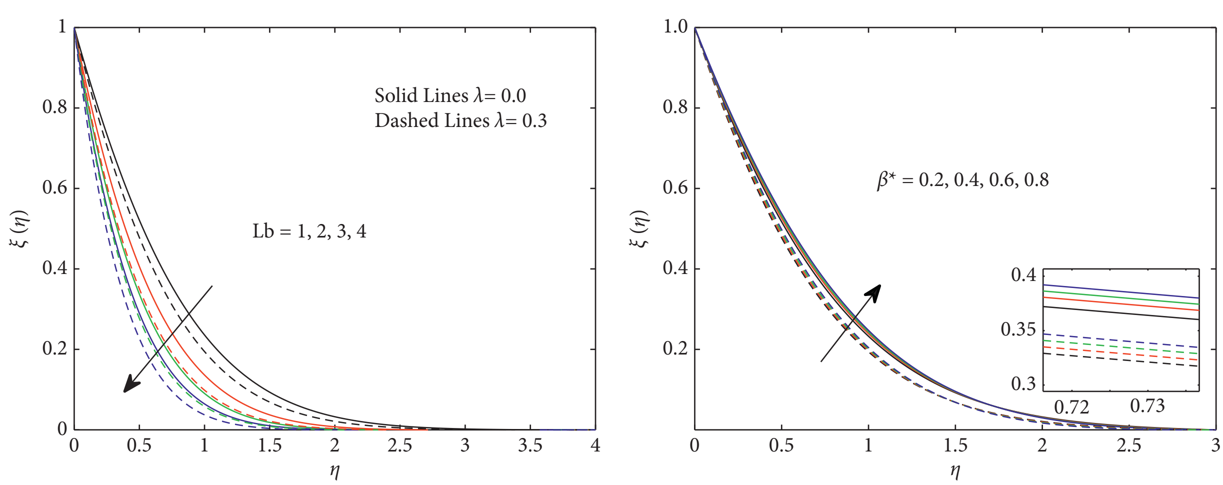

FIGURE 10: Variations due to (a) Lb and (b) β^* in $\xi(\eta)$.

Schmidt number Sc is upsurged, $\phi(\eta)$ is diminution. It is due to the fact that the mass diffusivity has inverse relation with the Schmidt number, therefore, the higher values of the Schmidt number bring weaker mass diffusion as a result nanoparticles concentration is dropped.

5.5.4. The Density Profile. The behavior of the motile density profile $\xi(\eta)$ due to emerging parameters is displayed in Figures 9(a), 9(b), 10(a), and 10(b). A diminution in motile density profile $\xi(\eta)$ is noticed as the unsteadiness parameter A is upsurged; however, it is mounted for an increment in the Hartree pressure gradient β as presented in Figures 9(a) and 9(b), respectively. A raise in bioconvection Lewis number Lb causes a decline in motile density profile $\xi(\eta)$ as portrayed in Figure 10(a). Physically, the diffusivity of the organism decreases as bioconvection Lewis number Lb is enhanced due to which motile density distribution $\xi(\eta)$ and relevant boundary layer thickness are declined. The influence of micro-organism concentration difference parameter β^* on motile density profile $\xi(\eta)$ is demonstrated in Figure 10(b). The motile density distribution $\xi(\eta)$ is augmentation for growing values of micro-organism concentration difference parameter β^*. However, it is smaller in case of stretching wedge as compared with static wedge.

6. Conclusions

In the present article, numerical investigation of tangent hyperbolic nanofluid flow over a wedge-shaped surface in the presence of micro-organisms has been presented. Few of the important results are as follows:

(i) The skin friction is enhanced whereas the motile density number is vitiated for larger values of the Hartree pressure gradient β

(ii) The Nusselt number, skin friction coefficient, and Sherwood number are increased as the unsteadiness parameter A gets bigger

(iii) The velocity profile is increased for the growing values of the magnetic number M and the unsteadiness parameter A

(iv) The energy and concentration distribution are diminished for the escalating values of the unsteadiness parameter A

(v) The density field is attenuated as unsteadiness parameter A and the bioconvection Lewis number Lb are increased but reverse behavior is noticed for the micro-organism concentration difference parameter β^* and the Hartree pressure gradient β

Abbreviations

$A = c/ax^{m-1}$:	The unsteadiness parameter
B_0:	Applied magnetic field
C_∞:	Ambient concentration
C:	Boundary layer concentration
C_p:	Specific heat
C_f:	Skin friction coefficient
C_0:	Initial reference concentration
C_w:	Concentration at wall surface
D_T:	Thermophoresis diffusion parameter
D_B:	Brownian diffusion coefficient
$Ec = U_w^2/(C_p)_f(T_w - T_\infty)$:	Eckert number
h_w:	Local surface heat flux
n:	Thermal conductivity
Lb:	Bioconvection Lewis number
$M = \sigma B_0^2/a\rho xm - 1$:	Magnetic number
k:	The power law index
N:	Boundary layer micro-organism
N_0:	Initial micro-organism concentration
N_w:	Micro-organisms at wall surface
Nu_x:	Nusselt number
$Nt = \Lambda D_T(T_w - T_\infty)/\nu T_\infty$:	Thermophoresis parameter
$Nb = \Lambda D_B(C_w - C_\infty)/\nu$:	Brownian motion parameter
$Pr = \nu/\alpha$:	Prandtl number
$Pe = bW_c/D_n$:	The bioconvection Peclet number
$Rd = 4\sigma^* T_\infty^3/k\kappa^*$:	Thermal radiation parameter
q_r:	Radiative heat flux
$Sc = \nu/D_B$:	The Schmidt number
t:	Time
T_w:	Surface temperature
T:	Boundary layer temperature
T_0:	Initial reference temperature
kT_∞:	Ambient temperature
u, v:	Velocity components
u_w:	Characteristics velocity
$We = \sqrt{\Gamma^2(m+1)U_e^3/\nu x}$:	The Weissenberg number.

Greek Symbols

ν:	Kinematic viscosity
ρ:	Fluid density
μ:	Dynamic viscosity
σ_m:	Electric charge density
φ:	Dimensionless concentration
θ:	Dimensionless temperature
$(\rho C_p)_f$:	Heat capacity of the fluid
$(\rho C_p)_p$:	Heat capacity of the nanoparticles $\Lambda = (\rho C_p)_p/(\rho C_p)_f$
η:	Dimensionless boundary layer thickness
λ:	The velocity ratio parameter
$\beta = m/m + 2$:	Hartree pressure gradient
$\beta^* = N_\infty/N_w - N_\infty$:	Micro-organism concentration difference parameter.

Data Availability

No data were used to support this study.

Conflicts of Interest

The authors declare that they have no conflicts of interest.

References

[1] S. U. S. Choi, "Development and application of non-Newtonian flows," *American Society of Mechanical Engineers (ASME)*, vol. 231, pp. 99–105, 1995.

[2] S. Lee, S. U.-S. Choi, S. Li, and J. A. Eastman, "Measuring thermal conductivity of fluids containing oxide nanoparticles," *Journal of Heat Transfer*, vol. 121, no. 2, pp. 280–289, 1999.

[3] J. A. Eastman, S. U. S. Choi, S. Li, W. Yu, and L. J. Thompson, "Anomalously increased effective thermal conductivities of ethylene glycol-based nanofluids containing copper nanoparticles," *Applied Physics Letters*, vol. 78, no. 6, pp. 718–720, 2001.

[4] M. Sheikholeslami, S. A. Shehzad, Z. Li, and A. Shafee, "Numerical modeling for alumina nanofluid magnetohydrodynamic convective heat transfer in a permeable medium using Darcy law," *International Journal of Heat and Mass Transfer*, vol. 127, pp. 614–622, 2018.

[5] H. Goodarzi, O. A. Akbari, M. M. Sarafraz, M. M. Karchegani, M. R. Safaei, and G. A. Sheikh Shabani, "Numerical simulation of natural convection heat transfer of nanofluid with Cu MWCNT and Al_2O_3," *Journal of Thermal Science and Engineering Applications*, vol. 11, no. 6, 2019.

[6] H. Mondal, S. Mishra, P. K. Kundu, and P. Sibanda, "Entropy generation of variable viscosity and thermal radiation on magneto nanofluid flow with dusty fluid," *Journal of Applied and Computational Mechanics*, vol. 6, no. 1, pp. 171–182, 2020.

[7] T. Khamliche, S. Khamlich, T. B. Doyle, D. Makinde, and M. Maaza, "Thermal conductivity enhancement of nano-silver particles dispersed ethylene glycol based nanofluids," *Materials Research Express*, vol. 5, no. 3, Article ID 35020, 2018.

[8] Z. Nisar, T. Hayat, A. Alsaedi, and B. Ahmad, "Significance of activation energy in radiative peristaltic transport of Eyring-Powell nanofluid," *International Communications in Heat and Mass Transfer*, vol. 116, p. 104655, 2020.

[9] R. Ellahi, F. Hussain, S. Asad Abbas, M. M. Sarafraz, M. Goodarzi, and M. S. Shadloo, "Study of two-phase Newtonian nanofluid flow hybrid with Hafnium particles under the effects of slip," *Inventions*, vol. 5, no. 1, 2020.

[10] M. M. Sarafraz and F. C. Christo, "Phase change heat transfer induced by plasmon heat generation in liquid micro-layer inside a micro-reactor," *Journal of Energy Storage*, vol. 42, Article ID 103033, 2021.

[11] W. Ibrahim and A. Tulu, "Magnetohydrodynamic (MHD) boundary layer flow past a wedge with heat transfer and viscous effects of nanofluid embedded in porous media," *Mathematical Problems in Engineering*, vol. 2019, Article ID 4507852, 2019.

[12] S. M. Atif, S. Hussain, and M. Sagheer, "Heat and mass transfer analysis of time-dependent tangent hyperbolic nanofluid flow past a wedge," *Physics Letters A*, vol. 383, no. 11, pp. 1187–1198, 2019.

[13] D. Ibrahim, M. Daba, and S. Bati, "Optimal Homotopy asymptotic method for investigation of effects of thermal radiation, internal heat generation, and buoyancy on velocity and heat transfer in the Blasius flow," *Mathematical Problems in Engineering*, vol. 2021, Article ID 5598817, 2021.

[14] S. Yousefzadeh, H. Rajabi, N. Ghajari, M. M. Sarafraz, O. A. Akbari, and M. Goodarzi, "Numerical investigation of mixed convection heat transfer behavior of nanofluid in a cavity with different heat transfer areas," *Journal of Thermal Analysis and Calorimetry*, vol. 140, no. 6, pp. 2779–2803, 2020.

[15] S. M. Atif, S. Hussain, and M. Sagheer, "Effect of thermal radiation and variable thermal conductivity on magnetohydrodynamics squeezed flow of Carreau fluid over a sensor surface," *Journal of Nanofluids*, vol. 8, no. 4, pp. 806–816, 2019.

[16] C. S. Sravanthi and R. S. R. Gorla, "Effects of heat source/sink and chemical reaction on MHD Maxwell nanofluid flow over a convectively heated exponentially stretching sheet using homotopy analysis method," *International Journal of Applied Mechanics and Engineering*, vol. 23, no. 1, pp. 137–159, 2018.

[17] M. Raza, R. Ellahi, S. M. Sait, M. M. Sarafraz, M. S. Shadloo, and I. Waheed, "Enhancement of heat transfer in peristaltic flow in a permeable channel under induced magnetic field using different CNTs," *Journal of Thermal Analysis and Calorimetry*, vol. 140, no. 3, pp. 1277–1291, 2020.

[18] M. M. Sarafraz and F. C. Christo, "Thermal and flow characteristics of liquid flow in a 3D-printed micro-reactor: a numerical and experimental study," *Applied Thermal Engineering*, vol. 199, Article ID 117531, 2021.

[19] A. F. Elelamy, N. S. Elgazery, and R. Ellahi, "Blood flow of MHD non-Newtonian nanofluid with heat transfer and slip effects," *International Journal of Numerical Methods for Heat and Fluid Flow*, vol. 30, no. 11, pp. 4883–4908, 2020.

[20] S. M. Atif, A. Kamran, and S. Shah, "MHD micropolar nanofluid with non Fourier and non Fick's law," *International Communications in Heat and Mass Transfer*, vol. 122, Article ID 105114, 2021.

[21] S. Chakraborty and P. K. Panigrahi, *Stability of Nanofluid: A Review*, Applied Thermal Engineering, Amsterdam, Netherlands, 2020.

[22] S. Nazari, R. Ellahi, M. M. Sarafraz, M. R. Safaei, A. Asgari, and O. A. Akbari, "Numerical study on mixed convection of a non-Newtonian nanofluid with porous media in a two lid-driven square cavity," *Journal of Thermal Analysis and Calorimetry*, vol. 140, no. 3, pp. 1121–1145, 2020.

[23] S. M. Atif, M. Abbas, U. Rashid, and H. Emadifar, "Stagnation point flow of EMHD micropolar nanofluid with mixed convection and slip boundary," *Complexity*, vol. 2021, Article ID 3754922, 2021.

[24] M. Y. Malik, T. Salahuddin, A. Hussain, and S. Bilal, "MHD flow of tangent hyperbolic fluid over a stretching cylinder: using Keller box method," *Journal of Magnetism and Magnetic Materials*, vol. 395, pp. 271–276, 2015.

[25] R. Ellahi, S. Z. Alamri, A. Basit, and A. Majeed, "Effects of MHD and slip on heat transfer boundary layer flow over a moving plate based on specific entropy generation," *Journal of Taibah University for Science*, vol. 12, no. 4, pp. 476–482, 2018.

[26] K. Jabeen, M. Mushtaq, and R. M. Akram, "Analysis of the MHD boundary layer flow over a nonlinear stretching sheet in a porous medium using semianalytical approaches," *Mathematical Problems in Engineering*, vol. 2020, Article ID 3012854, 2020.

[27] M. Ramzan, H. Gul, J. D. Chung, S. Kadry, and Y.-M. Chu, "Significance of Hall effect and Ion slip in a three-dimensional bioconvective tangent hyperbolic nanofluid flow subject to Arrhenius activation energy," *Scientific Reports*, vol. 10, no. 1, pp. 18342–18357, 2020.

[28] P. P. Gharami, S. Reza-E-Rabbi, S. M. Arifuzzaman, M. S. Khan, T. Sarkar, and S. F. Ahmmed, "MHD effect on unsteady flow of tangent hyperbolic nano-fluid past a moving

cylinder with chemical reaction," *SN Applied Sciences*, vol. 2, no. 7, p. 1256, 2020.

[29] A. Shafiq, S. A. Lone, T. N. Sindhu, Q. M. Al-Mdallal, and G. Rasool, "Statistical modeling for bioconvective tangent hyperbolic nanofluid towards stretching surface with zero mass flux condition," *Scientific Reports*, vol. 11, no. 1, pp. 13869–13880, 2021.

[30] M. A. Yousif, H. F. Ismael, T. Abbas, and R. Ellahi, "Numerical study of momentum and heat transfer of MHD Carreau nanofluid over an exponentially stretched plate with internal heat source/sink and radiation," *Heat Transfer Research*, vol. 50, no. 7, pp. 649–658, 2019.

[31] S. Shah, S. M. Atif, and A. Kamran, "Radiation and slip effects on MHD Maxwell nanofluid flow over an inclined surface with chemical reaction," *Heat Transfer*, vol. 50, no. 4, pp. 4062–4085, 2021.

[32] S. Rashidi, M. Dehghan, R. Ellahi, M. Riaz, and M. T. Jamal-Abad, "Study of stream wise transverse magnetic fluid flow with heat transfer around an obstacle embedded in a porous medium," *Journal of Magnetism and Magnetic Materials*, vol. 378, pp. 128–137, 2015.

[33] S. M. Atif, S. Hussain, and M. Sagheer, "Effect of viscous dissipation and Joule heating on MHD radiative tangent hyperbolic nanofluid with convective and slip conditions," *Journal of the Brazilian Society of Mechanical Sciences and Engineering*, vol. 41, no. 4, pp. 189–206, 2019.

[34] R. Ellahi, R. S.U., S. Nadeem, and V. K, "The blood flow of Prandtl fluid through a tapered stenosed arteries in permeable walls with magnetic field," *Communications in Theoretical Physics*, vol. 63, no. 3, pp. 353–358, 2015.

[35] M. S. Kandelousi and R. Ellahi, "Simulation of ferrofluid flow for magnetic drug targeting using the lattice Boltzmann method," *Zeitschrift für Naturforschung A*, vol. 70, no. 2, pp. 115–124, 2015.

[36] Z. Ullah, G. Zaman, and A. Ishak, "Magnetohydrodynamic tangent hyperbolic fluid flow past a stretching sheet," *Chinese Journal of Physics*, vol. 66, pp. 258–268, 2020.

[37] S. M. Atif, S. Hussain, and M. Sagheer, "Numerical study of MHD micropolar Carreau nanofluid in the presence of induced magnetic field," *AIP Advances*, vol. 8, 2018.

[38] H. Xu and J. Cui, "Mixed convection flow in a channel with slip in a porous medium saturated with a nanofluid containing both nanoparticles and microorganisms," *International Journal of Heat and Mass Transfer*, vol. 125, pp. 1043–1053, 2018.

[39] D. Pal and S. K. Mondal, "Influence of chemical reaction and nonlinear thermal radiation on bioconvection of nanofluid containing gyrotactic microorganisms with magnetic field," *BioNanoScience*, vol. 8, no. 4, pp. 1065–1080, 2018.

[40] S. M. Atif, S. Hussain, and M. Sagheer, "Magnetohydrodynamic stratified bioconvective flow of micropolar nanofluid due to gyrotactic microorganisms," *AIP Advances*, vol. 9, 2019.

[41] M. Zhao, Y. Xiao, and S. Wang, "Linear stability of thermal-bioconvection in a suspension of gyrotactic micro-organisms," *International Journal of Heat and Mass Transfer*, vol. 126, pp. 95–102, 2018.

[42] S. Saini and Y. D. Sharma, "Analysis of onset of bio-thermal convection in a fluid containing gravitactic microorganisms by the energy method," *Chinese Journal of Physics*, vol. 56, no. 5, pp. 2031–2038, 2018.

[43] K. Al-Khaled, S. U. Khan, and I. Khan, "Chemically reactive bioconvection flow of tangent hyperbolic nanoliquid with gyrotactic microorganisms and nonlinear thermal radiation," *Heliyon*, vol. 6, 2020.

[44] S. Sarkar and M. F. Endalew, "Effects of melting process on the hydromagnetic wedge flow of a Casson nanofluid in a porous medium," *Boundary Value Problems*, vol. 43, 2019.

[45] C. S. K. Raju, M. M. Hoque, and T. Sivasankar, "Radiative flow of Casson fluid over a moving wedge filled with gyrotactic microorganisms," *Advanced Powder Technology*, vol. 28, no. 2, pp. 575–583, 2017.

[46] E. Fatunmbi and A. Adeniyan, "MHD stagnation point-flow of micropolar fluids past a permeable stretching plate in porous media with thermal radiation, chemical reaction and viscous dissipation," *Journal of Advances in Mathematics and Computer Science*, vol. 26, no. 1, pp. 1–19, 2018.

[47] K. G. Kumar, B. J. Gireesha, and R. S. R. Gorla, "Flow and heat transfer of dusty hyperbolic tangent fluid over a stretching sheet in the presence of thermal radiation and magnetic field," *International Journal of Mechanical and Materials Engineering*, vol. 13, 2018.

[48] K. R. Rajagopal, A. S. Gupta, and T. Y. Na, "A note on the Falkner-Skan flows of a non-Newtonian fluid," *International Journal of Non-linear Mechanics*, vol. 18, no. 4, pp. 313–320, 1983.

[49] B. L. Kuo, "Application of the differential transformation method to the solutions of Falkner-Skan wedge flow," *Acta Mechanica*, vol. 164, no. 2-3, pp. 161–174, 2003.

[50] A. Ishak, R. Nazar, and I. Pop, "Falkner-Skan equation for flow past a moving wedge with suction or injection," *Journal of Applied Mathematics and Computing*, vol. 25, no. 1-2, pp. 67–83, 2007.